Talanta 300 (2026) 129198

Contents lists available at ScienceDirect

Talanta

journal homepage: www.elsevier.com/locate/talanta

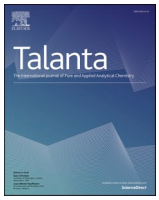

Colorimetric sensing for transdermal phospho-Tau 181 detection mediated by wearable microneedle functionalized with gold nanoparticle (MN-AuNP)

Anna Palma [a], Concetta Di Natale [b,*], Daniele Tammaro [b], Elena Lagreca [d], Gennaro Giordano [a], Simone Russo [b], Giuseppe Vitiello [b], Vincenzo Ferraro [c], Veronica Vespini [a], Simonetta Grilli [a], Pier Luca Maffettone [b], Sara Coppola [a,**]

[a] Institute of Applied Sciences and Intelligent System (CNR-ISASI), Via Campi Flegrei 34, 80078, Pozzuoli, (NA), Italy
[b] Department of Chemical, Materials, and Industrial Production Engineering (DICMaPI), University of Naples Federico II, 80125, Naples, Italy
[c] Department of Engineering and Architecture, University of Parma, Via delle Scienze 181, 43124, Parma, Italy
[d] Center for Advanced Biomaterials for Healthcare (IIT@CRIB), Istituto Italiano di Tecnologia, argo Barsanti e Matteucci 53, 80125, Napoli, Italy

ARTICLE INFO

Keywords:
Colorimetric sensing
Microneedle device
AuNPs coating
Wearable sensor

ABSTRACT

Microneedles (MNs) have rapidly emerged as powerful tools in wearable biosensing, providing minimally invasive access to interstitial fluid (ISF). Among the neurodegenerative based biomarkers detectable in ISF, phosphorylated Tau at threonine 181 (p-Tau181) is reaching a clinically evaluable significance for Alzheimer's disease (AD) and other tauopathies. Elevated p-Tau181 levels are strongly correlated with abnormal Tau aggregation in the brain and with cognitive decline. Current diagnostic methods rely on invasive cerebrospinal fluid (CSF) sampling or costly laboratory immunoassays and radio-imaging which are unsuitable for routine or point-of-care screening. Here, we present a highly sensitive colorimetric microneedle-based immunosensor designed for non-invasive, transdermal detection of p-Tau181. For the first time, gold nanoparticles (AuNPs) are integrated into a three-dimensional (3D) microneedle geometry, where antibody antigen recognition occurs directly on MN in contact with ISF. The aggregation-induced optical shifts of AuNPs provide an immediate and instrument-free colorimetric signal, while two optimized coating techniques enable uniform immobilization and reproducible performance. The MN-AuNP platform achieves a limit of detection (LoD) of 16 pg/mL, a nearly 30-fold improvement compared to the reported 2D surface (460 pg/mL). This enhancement shoots from the 3D architecture, which offers greater surface area, enhanced probe loading, and improved analyte diffusion. Compared with existing diagnostic approaches, the proposed system offers multiple advantages: non-invasive operation, real-time readout without complex instrumentation, low fabrication cost, and potential integration into wearable or point-of-care formats. Collectively, these results lay the groundwork for advanced MN-based colorimetric biosensors for early Alzheimer's disease detection through accessible and patient-friendly neurodiagnostic technologies.

1. Introduction

Colorimetric detection methods represent low-cost and rapid diagnostic systems compared to conventional methods and are known as a powerful platform for multiple diagnostics of biomarkers. The primary source of protein-related biomarkers is bodily fluids like blood or plasma, but sampling these fluids has drawbacks such patient accessibility issues or time-consuming laboratory procedures [1]. Non-invasive sensors based on urine, tears, or saliva have been developed to get over these problems, however they have low-slung diagnostic value and have limits regarding biomarker concentration and poor correlation with blood [2]. Interstitial fluid (ISF) is an interesting source of biomarkers (~80), many of which are highly correlated with blood, and some of them are exclusive to certain diseases such as

* Corresponding author.
** Corresponding author.
E-mail addresses: concetta.dinatale@unina.it (C. Di Natale), sara.coppola@isasi.cnr.it (S. Coppola).

https://doi.org/10.1016/j.talanta.2025.129198
Received 16 September 2025; Received in revised form 27 November 2025; Accepted 29 November 2025
Available online 2 December 2025
0039-9140/© 2025 The Authors. Published by Elsevier B.V. This is an open access article under the CC BY-NC-ND license (http://creativecommons.org/licenses/by-nc-nd/4.0/).

melanoma or squamous cell skin carcinoma [3,4]. Furthermore, ISF can be useful for continuous biomolecule monitoring (e.g. in chronic diseases) due to its absence of clotting factors[5–7]. Conversely, by reason of the stratum corneum barrier presence, ISF biomarkers can hardly permeate the skin layers and are difficult to be detected [8,9]. To date, ISF is collected using open-flow microperfusion or microdialysis; however, these techniques demand skilled training and local anesthetic with high risks for nosocomial infections [10,11]. To allow the clinical use of ISF as a diagnostic fluid, a straightforward and less invasive collection technique is required. In this context, microneedles (MNs) could represent a valid approach [12,13]. Recently, colorimetric microneedle patches have been proposed as efficient diagnostic methods for detecting high blood sugar levels. Gold nanoparticle-based functionalized microneedles have been tested for screening glucose concentrations, and silica nanoparticle-based photonic crystal microneedle arrays have been proved for the detection of wound inflammation-related biomarkers, (i.e. pH, glucose, and histamine) [14]. Zhao et al. successfully developed swellable hydrogel microneedles composed of polyvinyl alcohol and sodium alginate using chemical cross-linking (polyvinyl alcohol/SA) and extracted 6.4 mg of skin ISF in 15 min, then used it to recover and detect biomarkers such as glutathione (GSH) [15]. These devices are indeed minimally invasive for biomarker transdermal microsampling and have demonstrated great potential for extracting and detecting target analytes in ISF [9,16,17]. With benefits like self-application by little discomfort and invasiveness, MNs with heights of 100–1500 μm can pierce an epidermal layer that is 50–200 μm thick to remove ISF from the dermis, which is located under the stratum corneum layer with a thickness from 1500 to 3000 μm [18,19]. Additionally, by integrating MNs with various sensing technologies, a robust and reliable system can be created to support timely patient health diagnosis[17,20–25]. In fact, utilizing microneedle patches that employ color changes represents a key enabling technology for painless and straightforward method for detecting transdermal biomarkers improving overall patient compliance [26]. Whitin this framework, this study developed an MN-based sensor to enhance Point-of-Care Testing (POCT) based on colorimetry. The results appeared very competitive when compared with innovative colorimetric biosensors based on different technologies (Table 1). In fact, our system provided compactness, portability, with a straightforward visual readout, and user-friendliness approach, simplifying the steps required for signal functionalization, read out and analysis. Specifically, by using gold nanoparticles (AuNPs) as sensing elements, we were able to take advantage of their ability to assemble or disassemble in response to different biomolecules adhering to or conjugating with MNs surface, forming strong bonds with the target analyte and ensuring the sensitivity of common colorimetric assays. AuNPs have been widely employed in colorimetric sensing platform due to their unique localized surface plasmon resonance (LPPR) properties, which enable sensitive optical responses to variation in the surrounding environment. When specific target interactions induce nanoparticle aggregation, the plasmon band shifts toward longer wavelengths, resulting in a blue or purple appearance [27]. This concept was based on our recent approach proposed for the polymeric 2D surface of a thin-film biosensor to selectively capture Tau protein [28,29], which was then transferred to the functionalization of polymeric three-dimensional microstructures. The MNs fabricated by micro-moulding technology and functionalized with two coating techniques with uniform immobilization and reproducible performance, have been extensively characterized in terms of morphology, mechanical and chemical properties. As proof of concept, this colorimetric-based sensor was tested to detect the phosphorylated Tau181 protein (phospho-Tau181 or p-Tau181), recently discovered in skin, as specific biomarker for Alzheimer's diseases (AD), and adopted for effective discrimination between AD pathologies and other tauopathies [30,31]. We demonstrated a highly sensitive response to the presence of p-Tau181, when detected by the MNs device using a sandwich-like immunosensor architecture and achieving a limit of detection (LoD) of 19 pg/mL and limit of quantification (LoQ) of 57 pg/mL. Considering a future where colorimetric point-of-care devices would be central to diagnostics, the obtained results could mark a significant step forward in microneedle-based colorimetric sensing for transdermal diagnostic applications.

2. Results and discussion

2.1. Design of the colorimetric MN biosensor

Gold nanoparticles were produced following a previously described method [29,36]. The AuNPs suspension was characterized in terms of size distribution and polydispersityindex (PDI) by Dynamic Light Scattering (DLS) and Transmission Electron Microscopy (TEM) [27]. The results of the characterization ensured good quality of the synthesis and the AuNPs were used for the first time to functionalize solid MN matrices, following the steps shown in Fig. 1A–C. In detail, bare PLGA matrices were chemically activated through a conventional EDC/NHS reaction (milliQ water, 0.1 M and 0.2 M respectively) [37]. This step was necessary to promote the covalent attachment between the PLGA's carboxylic groups and the p-Tau181 primary antibody (1:1000, PBS 1X, Ph 7.4, 4 °C overnight). Then, AuNPs (0.5 %, hexane) were deposited following two different coating techniques, that were a deep wetting method of complete submersion into the nanoparticles' suspension (DW), and a more localized method of drop casting (DC), in which only small droplets of liquid were used. The two different AuNP coating strategies were investigated to optimize surface coverage, analyte

Table 1
Comparison cost versus other reported colorimetric sensors.

Method/Platform	Reference (DOI)	Biomarker	LOD	Estimated Cost per Test (€)	Cost rationale/Notes
3D microneedle-based colorimetric sensor (drop-cast)	This work (3D MN configuration)	phospho-Tau 181	16 pg/mL	0.5–1.0	Minimal reagents, no washing steps, direct ISF contact; scalable and low cost.
2D polymeric film colorimetric sensor (planar surface)	10.1016/j.jcis.2024.08.201 [29]	tau	460 pg/mL	1.0–1.5	Low reagent consumption, simple planar fabrication, standard AuNP coating.
Dual-mode magnetic immunosensor (colorimetric & SERS)	10.1016/j.bios.2022.114935 [32].	p-tau396,404	24 pg/mL (colorimetric mode)	5–12	Magnetic beads, dual enzyme labels, colorimetric SERS readout instrumentation.
Apta-blot assay for p-tau231 (fluorescence and colorimetric)	10.3390/biomedicines10010093 [33]	p-tau231	4.71 pg/mL	3–8	Multiple incubation steps, blot membrane, aptamer labeling and wash cycles, digital camera
Wrist-worn microneedle nanozyme colorimetric biosensor	10.1016/j.snb.2024.136731 [34]	oxalate	0.897 μM (~104 pg/mL)	2–4	Redox-induced visible color change, minimally invasive ISF monitoring, moderate fabrication cost.
Microneedle patch integrated with distance-based paper analytical device	10.1039/d4lc00983e [35]	cortisol and dopamine	0.25 μg/mL for cortisol, 1.0 ng/mL for dopamine	1–10	Wearable device, on-site and simultaneous detection of two analytes.

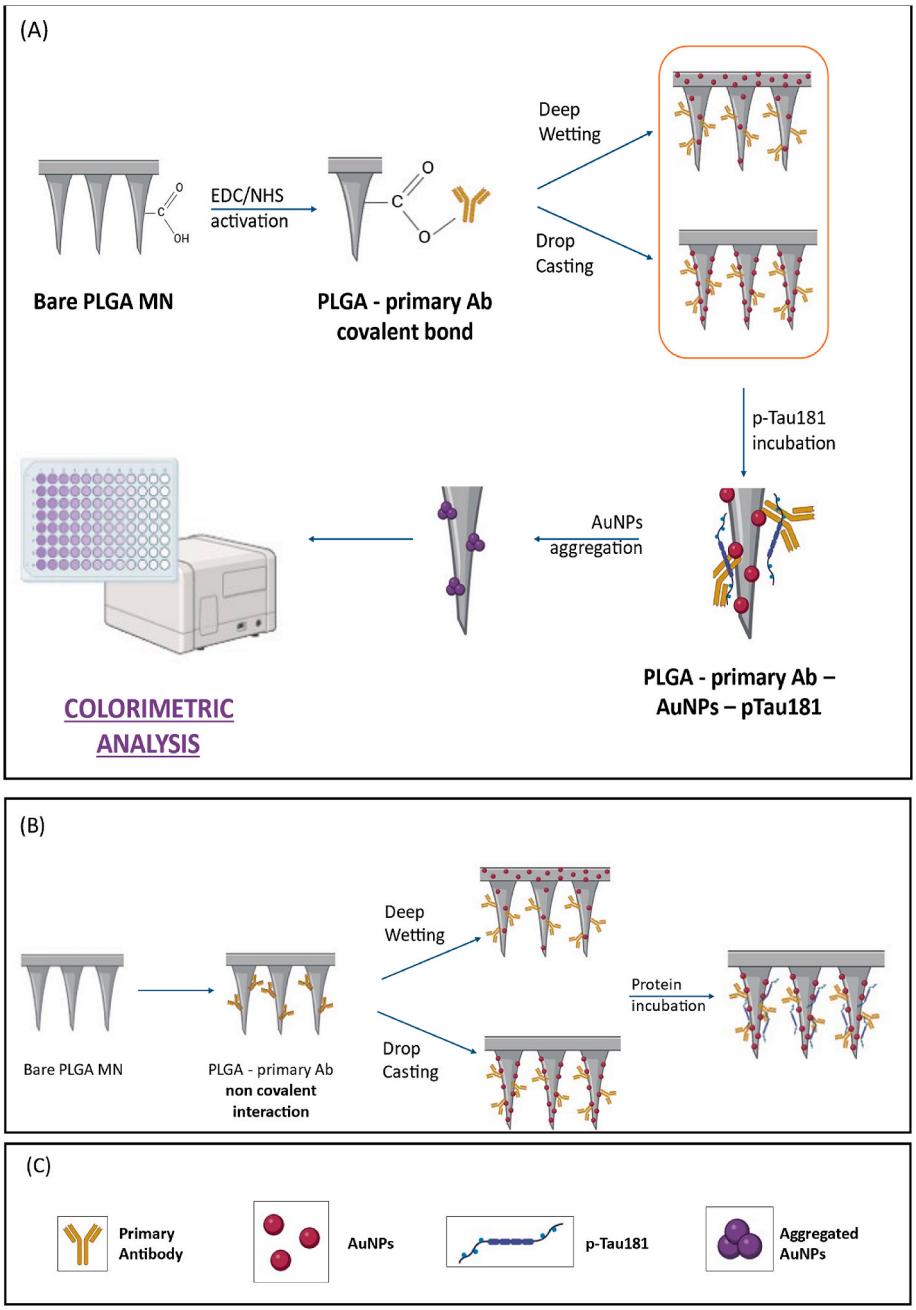

Fig. 1. A) Schematic illustration of all the chemical steps for the functionalization of treated PLGA MN matrices. B) preparation of control groups. C) legend of icons. Illustration was made by BioRender, free version.

accessibility, signal uniformity and material's consumption. Both techniques allowed the deposition of a thin monolayer of particles on the external surface of MNs. Regarding the deep wetting functionalization, the matrices were submerged in 1 mL of AuNPs suspension and gently stirred for 2 h, while for the drop casting droplets of 100 µL were directly released onto the outer surface of the matrices. In both cases, the samples were left under a fume hood after AuNPs deposition until complete hexane evaporation. Subsequently, 100 µL droplets of p-Tau181 solutions at six different concentrations in the picogram range were added to the final biosensor. After 15 min of reaction at ambient conditions, the color variation was quantitatively evaluated. Control formulations were also prepared using chemically inactive PLGA MNs. Potential interferent effects were evaluated by adding BSA and TNF-α proteins at a fixed concentration of 500 pg/mL while varying the concentration of p-Tau181, as described above.

2.2. Morphological characterization: stereomicroscopy, SEM and EDX analysis

Before the preparation of the colorimetric biosensor, each sample was observed by stereomicroscope. From this characterization, the successful replication of the master geometry through the micro-moulding process was confirmed (Fig. S1). The average height of the needles was 300 µm, with a center-to-center distance of 500 µm. The overall diameter of the circular matrixes was 1 cm and reflected the dimension of the mould. The good quality of the manufacturing process was also validated through SEM analysis. Micrographs reported in Fig. 2A and B display a well-defined microneedle array characterized by good uniformity in shape and size. Each microneedle exhibited a similar conical structure with regular sharps and tips. The base of each needle was fully integrated with the substrate, ensuring the final structural

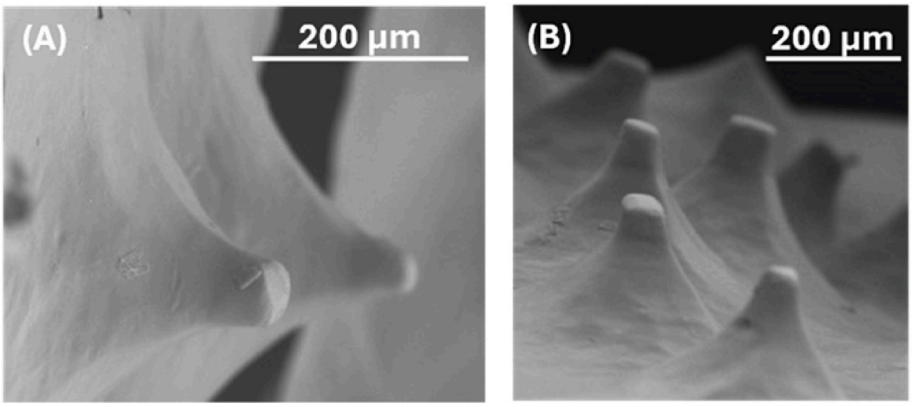

Fig. 2. (A)–(B) SEM micrographs of bare PLGA MNs at 200 µm magnification.

stability. After AuNPs deposition and drying at ambient temperature, the biosensor was ready for use. A SEM analysis was performed to observe the AuNPs distribution and compare drop-cast and deep-wet samples. Micrographs at different scale bars of the two groups are shown in Fig. 3 (from A to C PLGA-Ab-DW and from D to F PLGA-Ab-DC). From the SEM analysis, it appeared that the drop-casting method resulted in a more localized distribution, with AuNPs along the MNs body. Conversely, with the deep-wetting method, the dispersion of the particles was less selective, resulting in an increased AuNPs deposition in the spaces between the needles along the matrix, as clear in Fig. 3A and B. In combination with the SEM analysis, the EDX test was also performed. For the drop-casting method, the gold percentage was entirely concentrated on the needles; in fact, no gold was detected in space between them. Conversely, in the deep-wetting method, the element was more widely dispersed and detected in multiple areas, with a significantly lower percentage along the needles (see Supplementary, figure S2 A-B-C). This was probably because the submersion carried out for deep-wetting led to a more uniform coverage of the matrix, while drop-casting resulted in a more pronounced deposition of on the most exposed surfaces, that was the MN external surface. Furthermore, the EDX mapping revealed that gold was more concentrated on the needles than on the matrix, even when comparing the PLGA-DC (without antibody functionalization) and PLGA-Ab-DC samples, suggesting that the presence of cysteine residues from the antibody on the needle enhances the interaction with the nanoparticles (Figure S2 D–G). Finally, the EDX analysis of the PLGA-Ab-DC also detected the presence of sulfur and nitrogen, confirming the successful functionalization of the needles with the antibody (Figure S2 H). The real 3D structure of the microneedles was reconstructed in MATLAB to highlight the key characteristics of the MNs, offering, in conjunction with the microscopic characterization, a clear and intuitive view of their design and orientation in 3D space (see Supplementary File for details, Fig. S3).

2.3. *Mechanical properties: indentation test in vitro*

Owing to their viscoelastic properties that closely resemble those of human skin, agarose gels were utilized in this study as a biomimetic substrate for *in vitro* microneedle (MN) insertion testing. Although the mechanical properties of agar gels depend strongly on preparation conditions and testing methodology, measurements for 3 % w/w agar gels have been reported to exhibit Young's moduli in the range of approximately 50–150 kPa [38]. In comparison, in-vivo measurements of human skin yield Young's moduli of approximately 100–130 kPa [39]. Therefore, the 3 % agar formulation was selected as a suitable

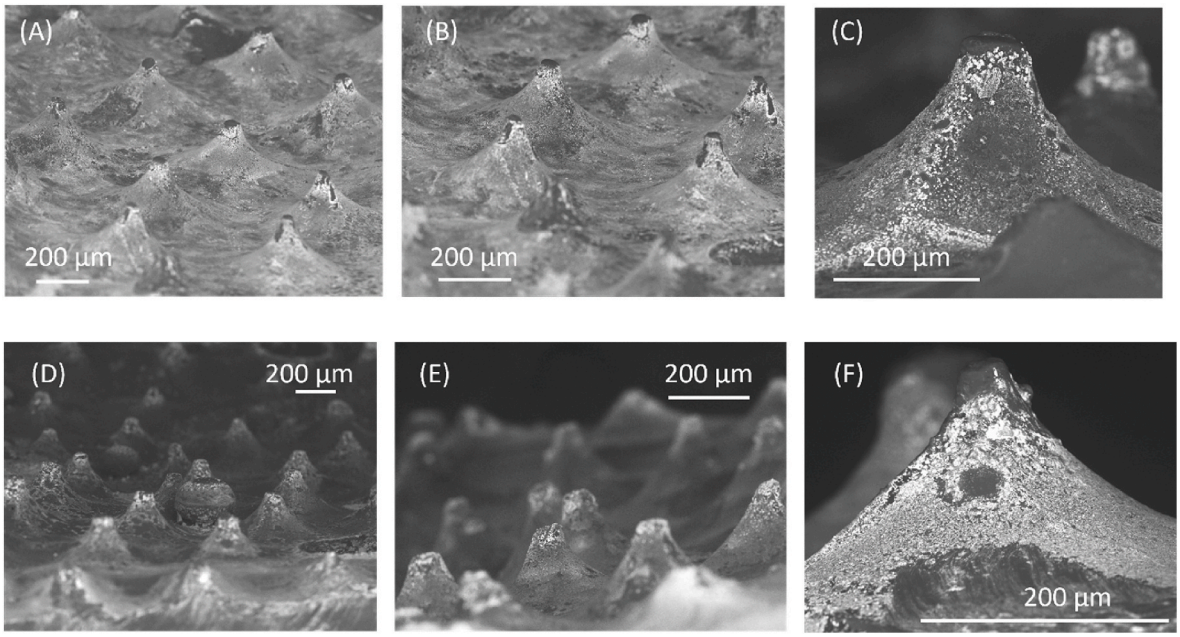

Fig. 3. (A)–(C) Micrographs of the PLGA-Ab-Deep Wetting matrix. (D) to (F) Micrographs of the PLGA-Ab-Drop Casting matrix. The different scale bars are reported on the images.

skin-mimetic substrate for our experiments. Firstly, bare PLGA and PLGA-Ab samples were tested to verify if the covalent attachment of the antibody had compromised the mechanical properties. The matrix was slowly driven towards a small piece of gel at a constant speed through a Microtest 200 N stages (Deben, UK). The registered data during insertion showed a very similar trend for both PLGA and PLGA-Ab, proving that no significant mechanical modifications occurred (results are shown in Supplementary File, Fig. S4). In light of these considerations, the coated samples (being PLGA-Ab-DW and PLGA-Ab-DC) were tested under predefined conditions. From the analysis of the experimental results, it was clear that, once MNs touched the gel, the force increased as function of the displacement at a certain slope (about 0.1 N/mm). After reaching a value of 0.15 N approximately, the force continued to increase at a lower growth rate, about 0.03 N/mm (Fig. 4); this behavior was probably due to the decrease in resistance of the gel, which began to yield under compression. No appreciable differences between the two systems were recorded, demonstrating that AuNP coating did not influence the MNs mechanical strength.

2.4. MNs penetration in 3D collagen matrix

Confocal laser scanning microscopy confirmed the efficient insertion of 300 μm microneedles loaded with rhodamine dye into the 400 μm-thick 3D collagen matrix (Figure S5 A-B). Z-stack reconstructions and 3D rendering enabled precise visualization of the MN profile (Figure S6 D) and the local deformation of the surrounding collagen fibers following insertion (Figure S6 A-B-C). The rhodamine channel clearly outlined the MN shaft, while the SHG signal revealed the collagen fibrillar network and its rearrangement around the insertion site. The intrinsic PLGA autofluorescence detected in the SHG signal further confirmed the localization of the MN tip within the matrix. After 30 min from implantation, rhodamine diffusion within the collagen was evident, suggesting progressive dye release and interaction with the fibrillar structure. Z-stack analysis indicated penetration depths of approximately 250 μm (Movie 1, 3D reconstruction of the collagen Z-stack after 30 min of needle indentation). These findings confirmed the effective penetration capability of our 300-μm high PLGA MNs in a 3D collagen matrix as a physiologically relevant platform.

Supplementary data related to this article can be found online at https://doi.org/10.1016/j.talanta.2025.129198.

2.5. AuNPs release studies and cell viability

To study whether the adsorption of the AuNPs was stable enough to prevent their release in a physiological environment, the matrices were suspended in PBS and incubated for several days at 37 °C, then the suspending fluid was analyzed by UV–Vis spectroscopy at different time points (1h, 2h, 24h, 48h, 7 days, 15 days, 21 days). The absorbance value of the spectra at 520 nm was read, as it typically corresponds to the localized surface plasmon resonance (LSPR) of monodisperse gold nanoparticles with a size between 15 and 20 nm. Control measurement was realized analyzing PLGA-Ab system. For each formulation, all the spectra were practically overlapping at each experimental time points. Moreover, the overlap also occurred between the functionalized microneedles and the control ones, demonstrating that the nanoparticles were stably adsorbed onto the polymer and were not released into the biological-like fluid. In the Supplementary File, as an example, the spectrum for the three systems at the longest incubation time, i.e., 21 days, has been provided (see Fig. S7). A Trypan Blue viability test was conducted to evaluate effects on SK-N-BE(2) neuroblastoma cell line. In Fig. 5 the percentage of cell viability is reported for the four groups of samples examined, referring to 24h of matrixes incubation. As it can be seen, no cytotoxic effects were caused by the presence of AuNPs. PLGA-Ab-DW showed a slight reduction in cell viability (nevertheless around 70 %) probably due to hexane residues resulting from the complete immersion of the matrices during sensor preparation. PLGA-Ab-DC, on which the deposition of nanoparticles yielded the best results, did not show any cytotoxic effects, confirming the potential use of the PLGA-Ab-AuNPs system for the realization of a wearable biosensor.

2.6. In vitro detection

The goal of the present work was to exploit the gold nanoparticles

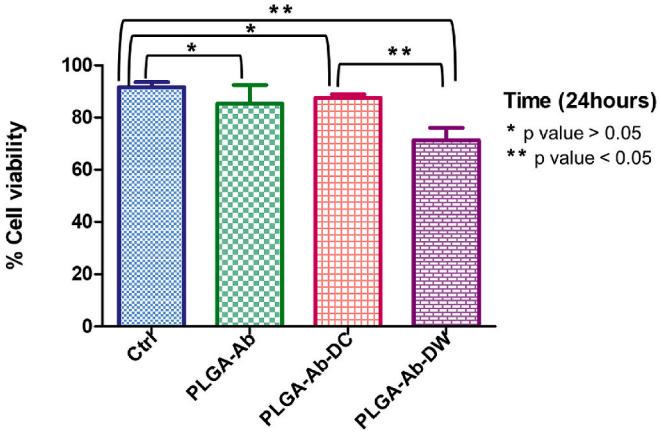

Fig. 5. Evaluation of SK-N-BE(2) neuroblastoma cells viability. Ctrl: cells without incubation of PLGA matrixes. Data are presented as (mean ± s.d.), n = 3.

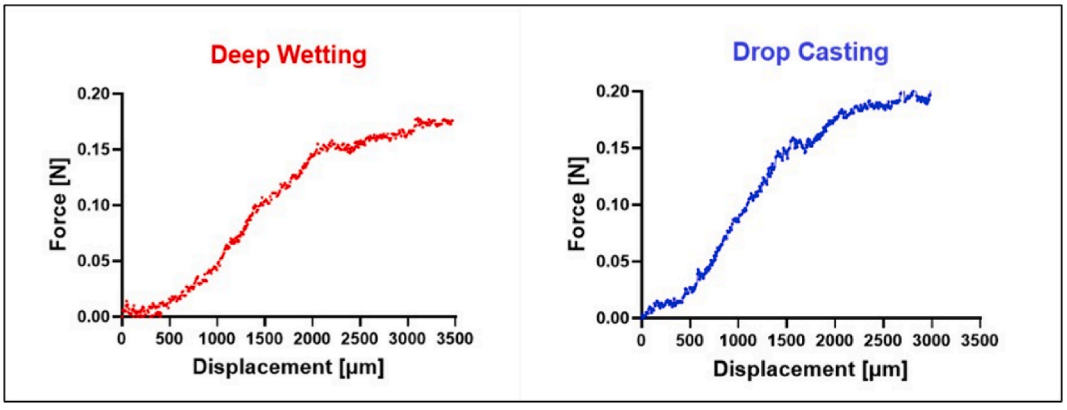

Fig. 4. Force vs displacement curves for PLGA-Ab-DW and PLGA-Ab-DC matrices obtained from insertion in agarose gels at test velocity of 1.5 mm/min; each matrix contained 100 microneedles.

aggregation induced by the formation of the antibody-antigen complexes sensing element. This phenomenon enhances the sensitivity of the sensor compared to common colorimetric sensors [40,41]. In a previous study, this possibility was already demonstrated using 2D structures (thin polymeric films) [29]. In the current study, the challenge was to transition to a more structurally complex system by fabricating MNs-based device, where antibody-antigen interactions occur on the 3D-conical structures. To the best of our knowledge, these two studies are the first attempts to apply a colorimetric test that exploits AuNPs aggregation in a dry environment. Typically, nanoparticle aggregation occurs in solution, where interactions are facilitated. In these two studies, NPs were suspended on a stiff surface, where their motility is reduced. Despite the challenge, the results demonstrated consistent and reproducible outcomes thus confirming that the AuNPs interactions were sufficient to induce aggregation and develop a MNs-based colorimetric biosensor. In this section, an analysis of the experimental results regarding the sensor characteristics is provided. PLGA-Ab-DC and PLGA-Ab-DW matrixes were utilized to evaluate the detection capabilities of the p-Tau181 protein in physiological-like conditions. The matrixes were incubated with known amounts of the analyte for 15 min, to promote AuNPs aggregation triggered by antibody-antigen interaction. The same protocol was applied to assess the effect of potential interferents by constructing a calibration curve at different p-Tau181 concentrations in the presence of 500 pg/mL of BSA and TNF-α. The color shift to dark red/purple was observed, typically associated with the aggregation of the AuNPs [27]. This change was noticeable not only under microscope (Fig. S8), but even to the naked eye (Fig. S9), with a more pronounced color variation for the drop-casted samples. As shown in Fig. 6A and B, the experimental data were well described by a four-parameter.

Logistic (4-PL) regression model, which captures saturation behavior and is commonly used to fit the nonlinear response typical of ELISA-like assays [42,43]. The coefficients of determination (R^2) were 0.981 for PLGA-Ab-DW, 0.998 for PLGA-Ab-DC, and 0.996 for PLGA-Ab-DC in presence of interferent species, indicating goodness of fit (see Table S2 for details). The Limit of Detection (LoD) and Limit of Quantification (LoQ) were calculated considering the initial range where the response was linear (Figure S10 A-B-C). Table 2 reports the parameters of the linear fit, as well as the LoD and LoQ values, showing lower limits for the drop-cast method. This confirmed the higher sensitivity previously hypothesized based on RGB signal analysis. In the presence of interferent species (BSA and TNF-α at 500 pg/mL), the LoD and LoQ increased to 69 pg/mL and 208 pg/mL, respectively. This rise can be attributed to the increased complexity of the matrix; nevertheless, both values remain within the picogram range, confirming the reliable performance of the system. Notably, the colorimetric response was unaffected by the interferents, and the MNs platform maintained satisfactory analytical performance even under more realistic conditions.

Table 2
Limit of detection (LoD) and limit of quantification (LoQ) obtained from the calibration curve for phospho-Tau181 detection in PBS, comparing two biosensor preparation methods.

Method	Intercept × 10	Slope × 10^3	LoD [pg/mL]	LoQ [pg/mL]
Deep Wetting	7.8 ± 0.4	−5.6 ± 0.7	23 ± 3	67 ± 8
Drop Casting	8.1 ± 0.3	−5.4 ± 0.5	19 ± 2	57 ± 6
Drop Casting + interferents	4.9 ± 0.5	−4.0 ± 1.0	69 ± 18	208 ± 50

These results indicate that both the deep wetting and drop-casting methods represent simple and effective strategies for functionalizing MN arrays to detect phospho-tau181. The deep-wetting method ensures a minor robust colorimetric uniformity, in contrast, drop casting maximizes the local density of recognition sites and enhances the biorecognition efficiency at the skin–sensor interface. Further considering potential large-scale production, the drop-casting method is preferable, as it yielded a biosensor with lower LoD and LoQ values compared to deep wetting, along with improved nanoparticle distribution and concentration across the needle bodies. This is further supported by its lower reagent consumption and shorter preparation time. Moreover, the observed improvement in the limit of detection (from 460 pg/mL for the 2D polymeric surface to 16 pg/mL for the microneedle-based sensor) can indeed be attributed to the transition from a 2D to 3D architecture. As widely reported in the literature [44,45], 3D microstructured interfaces, including microneedles, consistently yield superior sensitivity compared to planar configurations. This enhancement is primarily due to the increased effective surface area, higher probe density, and improved analyte diffusion and mass transport within the 3D geometry, which collectively contribute to a lower LOD.

3. Conclusion

This study successfully demonstrated the development of a MNs-based colorimetric sensor for the detection of p-Tau181, a neurodegeneration biomarker. Gold nanoparticles (AuNPs) were employed as sensing elements in the system, with their aggregation inducing color variations directly linked to the concentration of the target biomarker. Specifically, AuNPs were immobilized in dry conditions onto the complex geometry of microneedles using two different deposition methods: deep wetting and drop casting. In both preparations, morphological and mechanical analyses confirmed the structural stability of the sensor, ensuring good reproducibility. Stability studies proved that AuNPs remained firmly adsorbed on the MNs surface, with no release observed after several days of incubation. Cell viability assays demonstrated no

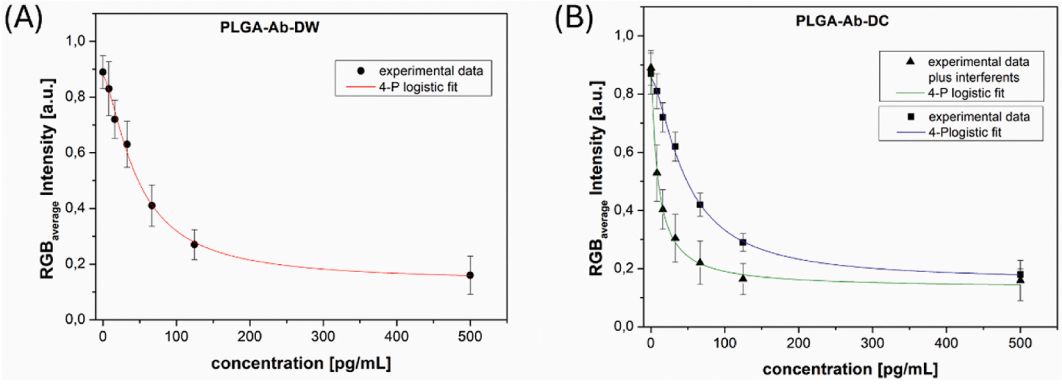

Fig. 6. (A), (B) Calibration curves of the signal as a function of analyte concentration. The data were fitted using the four-parameters logistic (4-PL) model, which provided a good description of the response behavior, including the observed saturation plateau for both PLGA-Ab-DW and PLGA-Ab-DC assays, even in presence of protein interferents. Fitting parameters are reported in the Supplementary File.

cytotoxic effects from PLGA matrixes functionalized with the p-Tau181 primary antibody and AuNPs. Anti-interference study with BSA and TNF-α proteins is reported. Among the two deposition strategies, drop-casting demonstrated advantages in terms of reduced reagents consumption, improved detection efficiency, and higher specificity, resulting in a limit of detection (LoD) of 19 pg/mL and a limit of quantification (LoQ) of 57 pg/mL, as determined from calibration curves generated in PBS to simulate physiological ambience. This highly competitive sensitivity arises from the larger effective surface area, direct access to interstitial fluid (ISF), improved mass transport, and volume-distributed catalytic sites provided by the 3D geometry. In our system, the color change observed in the drop-casting samples was more pronounced and clearly visible to the naked eye. This feature of the sensor has the potential to obviate the need for complex instrumentation, thereby enhancing the accessibility, cost-effectiveness, and practicality of the approach for on-site, real-time monitoring. The reported results mark a significant step toward the future of transdermal diagnostics and wearable healthcare technologies, offering new opportunities for point-of-care applications and personalized medicine. Future studies will focus on detecting the analyte in complex environments and performing the insertion of microneedles into real skin.

4. Experimental section

Reagents and Materials: Poly(lactic-co-glycolic acid) (PLGA RESOMER® RG 504H, 38000–54000 Da, lactide: glycolide = 50 : 50), dimethyl carbonate (DMC, 99 % v/v), N-(3-(dimethylamino)propyl)-N′-ethylcarbodiimide hydrochloride (EDC)/N-hydroxysuccinimide (NHS), Phosphate Buffered Saline (PBS 1X, pH 7.4), and Trypsin-EDTA 0.25 % Solution were all purchased from Merck/Sigma-Aldrich, Italy. DMEM high glucose, Ham's F12, FBS, 1 % Penicillin-Streptomycin solution 100X 6,0/10,0 g/L, 1 % L-Glutamine 100 × 200 mM were all purchased from Avantor, Radnor, PA, USA. Agar powder and Trypan Blue solution were purchased from Thermo Fisher Scientific, Cleveland, OH, USA. Ecoflex 00–50 (used for micro-moulds) was supplied by Smooth-On, Inc., Macungie, Pennsylvania, USA. The Tau phosphorylated at threonine-181 (p-Tau181) was purchased from Fujirebio, Japan, and the rabbit anti-Tau from Cell Signaling Technologies Rabbit D9F4G, Belgium. Bovine Serum Albumin (BSA, Sigma-Aldrich, Cat. No. A9418, St. Louis, MO, USA) and recombinant human TNF alpha protein (active) (ab259410, Abcam, UK) were used as protein interferents.

MNs matrices fabrication and characterization: All microneedles used in this work were fabricated using poly(lactic-co-glycolic acid) (PLGA), a material commonly used in medical and pharmaceutical applications [46]. The technique employed for the fabrication of a MNs' matrix was micro-moulding. The final matrices replicated the structure of commercially available master moulds, consisting of 100 metallic needles [47]. To replicate the desired geometry, negative moulds were first fabricated using EcoflexTM 00−50 (skin-safe) in a base-to-curing agent ratio of 1:1, which required 3 h of curing under ambient conditions. The negative moulds were then filled with the PLGA solution (DMC, 25 % w/v). After 24 h under a fume hood, the polymeric matrices were finally detached and stored for future use. Before functionalization, MNs morphology was characterized by a ZEISS Axio Zoom.V16 stereomicroscope. Also, micrographs of the external surface of matrices were taken using the Scanning Electron Microscope (SEM) Hitachi TM3000, following preparation protocols as previously reported [48,49].

Biosensor characterization: SEM and EDX: After each step of functionalization, samples were observed by SEM to analyze possible modifications of MNs' surface. Four main experimental groups were considered: bare PLGA MNs, PLGA MNs bound with primary antibody (PLGA-Ab), PLGA-Ab coated with AuNPs by drop casting (PLGA-Ab-DC), and PLGA-Ab coated by deep wetting (PLGA-Ab-DW). SEM micrographs were also useful for evaluating the distribution of the nanoparticles. In combination with SEM, further studies thanks to Energy Dispersive X-ray spectroscopy (EDX) Swift ED 3000 X-Stream module (Hitachi) were carried out. EDS mapping capability was also employed for characterization. This allowed for the detection of gold on the needles and in the space between them, as well as for a comparison of the deposition achieved through the two methods of AuNPs deposition.

Calibration curve, LoD and LoQ evaluation: Once the biosensor was prepared, a calibration curve was performed. Six solutions of the analyte at known concentrations were used, ranging from 8.0 pg/mL to 500.0 pg/mL, PBS 1X (for specific points of the calibration curve see Supplementary File, Table S1). 100 μL of each solution were drop-cast on MNs matrix (in duplicate). The system was incubated at ambient conditions for 15 min to allow colloid formations in AuNPs. Changes in colour were evident and could be observed by a conventional ZEISS Axio Imager. M1m microscope and quantified by Image J Software. In detail, images were taken in bright field; the area of interest was manually selected, and colour intensity was measured by Image J (Red, Green, Blue channels average (RGB)). The average RGB value was normalized according to a Min-Max approach, and each value (from 0 to 1) was plotted against the corresponding known amounts of the analyte. A nonlinear fit of the experimental data was performed using the four-parameters logistic model in OriginLab (free version). Then, Limit of Detection and Limit of Quantification were determined according to the ICH guideline as $\mathrm{LoD} = 3.3\,\sigma/s$, and $\mathrm{LoQ} = 10\,\sigma/s$, where σ and s are the standard deviation of the response and the slope of the regression curve in the linear range, respectively [50]. Control groups were subjected to the procedure described above, using the highest analyte concentration of 500 pg/mL.

AuNPs release test; cell viability test: Samples were suspended into PBS 1X (pH 7.4) and incubated at 37 °C for 1h, 2h, 24h, 48h, 7gg, 15gg, 21gg, simulating physiological ambient (Labnet International 222DS Benchtop Shaking Incubator). PLGA-Ab-DC and PLGA-Ab-DW, and bare PLGA as controls were used for these experiments. 1 mL of the suspending liquid was taken and refreshed at different times (30 min, 1 h, 2 h, 24 h, 48 h, 7 gg, 15 gg, 30 gg, 2 months). The collected supernatant was analyzed by UV–Vis spectrophotometry (Thermo Scientific Multiskan SkyHigh Microplate Spectrophotometer), and the characteristic AuNPs peak at 520 nm was registered. Moreover, a cell viability assay was performed using the same set of samples with the Trypan Blue exclusion method and the LUNA™ II Automated Cell Counter (Logos Biosystems), following a protocol previously reported [51]. SK-N-BE(2) neuroblastoma cells were seeded in a 24-well plate at a seeding density of 100.000 cells/well and incubated for 24h in complete medium consisting of 1:1 mixture of DMEM high glucose (Avantor) and Ham's F12 (Avantor) supplemented with 10 % heat-inactivated FBS (Avantor), 1 % Penicillin-Streptomycin solution 100X 6,0/10,0 g/L (Avantor), 1 % L-Glutamine, 100 × 200 mM (Avantor). After 24h, cells' medium was removed and the matrixes were applied into the wells, new fresh medium was then added, and the cells were incubated for an additional 24h. Following the incubation the samples were removed, and the cells harvested using Trypsin-EDTA 0.25 % Solution (Sigma-Aldrich) and resuspended in complete medium to obtain a uniform single-cell suspension. A 1:1 mixture of the cell suspension and 0.4 % Trypan Blue solution (Gibco, Thermo Fisher Scientific) was prepared. After a brief incubation of 2–3 min at room temperature, 10 μL of the stained suspension was loaded into a LUNA™ II reusable counting slide according to the manufacturer's instructions. The LUNA™ II device automatically discriminated viable (unstained) from non-viable (blue-stained) cells based on dye permeability and morphological characteristics, providing direct counts of live and dead cells, total cell concentration, and viability percentage. Statistical analysis and p value evaluation were performed using Prism graphPad version 8.

In vitro insertion test by SEM: A skin-mimicking gel based on agar powder was used as a model tissue for the insertion of MNs. The gel was prepared following a previously described protocol [52] using a 3 % mass concentration and kept at 4 °C and well-sealed with parafilm to avoid changes of humidity until use. The force and displacement of insertion were measured through a Microtest 200 N stages (Deben, UK).

Small pieces of the gel (2x2x1 cm) and MNs samples were placed in sample holders fabricated ad hoc using a 3D printer model I3 Mk3s from Prusa Research (Prague, Czech Republic). For each test, the speed at which the needles moved toward the gel was set at 1.5 mm/min, while the gel was held stationary. The insertion was recorded by a high-resolution frame rate camera.

MNs Collagen matrix penetration: To investigate the penetration capability of the MN array, a three-dimensional collagen gel was employed as a biomimetic matrix reproducing the mechanical and structural features of dermal tissue [46]. The 3D collagen matrix was prepared from non-peptonized rat-tail Collagen Type I (5 mg/mL, ibidi®, Gräfelfing, Germany), diluted to a final concentration of 4 mg/mL in cell culture medium (Dulbecco's Modified Eagle Medium, DMEM, Sigma-Aldrich, Milan, Italy) supplemented with 20 % FBS, 1 % glutamine, 1 % non-essential amino acids, and 100 U mL^{-1} penicillin, 100 mg/mL streptomycin. The collagen solution was actively mixed by pipetting to ensure homogeneity, and pH was adjusted by sequential addition of NaOH and sterile ultrapure water to a chilled sterile tube. The final mixture was gently homogenized and transferred into fluorodishes (μ-Dish 8 well, high Glass Bottom, ibidi®, Gräfelfing, Germany) within 5 min of preparation to avoid premature gelation. The samples were incubated at 37 °C in a 5 % CO_2 humidified atmosphere for 30 min to allow collagen fibrillogenesis. The formation and uniform distribution of collagen fibrils were confirmed by phase contrast microscopy and magnified 10x for fiber visualization. After gelation, the MNs patch embedding Rhodamine 6G (Dye content ~95 %, Merck/Sigma-Aldrich, Italy) was implanted into the collagen matrix under sterile conditions. The system was then imaged using a confocal laser scanning microscope, acquiring Z-stack images across the entire thickness of the gel. Images were obtained by confocal microscopy (Leica Microsystems TCS SP5 II, Germany) with a 25 × 45 N A. water immersion objective, and images were acquired with a resolution of 523 × 523 pixels. Fluorescent and structural signals were monitored through the rhodamine emission (microneedle), second harmonic generation (SHG) of the collagen fibers, and autofluorescence of the PLGA component. This experimental setup provides a controlled and reproducible platform to evaluate MN penetration dynamics and their spatial distribution within a dermal-like environment.

CRediT authorship contribution statement

Anna Palma: Writing – original draft, Investigation, Data curation. **Concetta Di Natale:** Writing – original draft, Investigation, Data curation, Conceptualization. **Daniele Tammaro:** Writing – review & editing, Investigation. **Elena Lagreca:** Investigation. **Gennaro Giordano:** Investigation. **Simone Russo:** Investigation. **Giuseppe Vitiello:** Writing – review & editing, Investigation, Conceptualization. **Vincenzo Ferraro:** Writing – review & editing, Methodology, Investigation. **Veronica Vespini:** Writing – review & editing, Methodology, Investigation. **Simonetta Grilli:** Writing – review & editing, Supervision, Conceptualization. **Pier Luca Maffettone:** Writing – review & editing, Supervision, Conceptualization. **Sara Coppola:** Writing – review & editing, Writing – original draft, Supervision, Funding acquisition, Conceptualization.

Declaration of competing interest

The authors declare the following financial interests/personal relationships which may be considered as potential competing interests: Sara Coppola reports financial support was provided by Ministry of Education and Merit. Pier Luca Maffettone reports financial support was provided by Italian Space Agency. If there are other authors, they declare that they have no known competing financial interests or personal relationships that could have appeared to influence the work reported in this paper.

Acknowledgements

We acknowledge financial support under the National Recovery and Resilience Plan (NRRP), Mission 4, Component 2, Investment 1.1, Call for tender No. 104 published on 2.2.2022 by the Italian Ministry of University and Research (MUR), funded by the European Union – NextGenerationEU– Project Title Microneedles Assisted photo-thermal therapy patch for minimally invasive nonmelanoma Skin cancer treatment (MASK) – CUP B53D23008670006- Grant Assignment Decree No. n. 966 adopted on 30/06/2023 by the Italian Ministry of Ministry of University and Research (MUR). This research was funded by the Italian collaborative agreement between the Italian Space Agency (ASI) and the University of Naples "Federico II" n. 2021-20-HH.0 on "Innovative Health Technology Development Activities in Space", Italian project code F65F21000830005.

Appendix A. Supplementary data

Supplementary data to this article can be found online at https://doi.org/10.1016/j.talanta.2025.129198.

Data availability

Data will be made available on request.

References

[1] G. He, T. Dong, Z. Yang, A. Branstad, L. Huang, Z. Jiang, Point-of-care COPD diagnostics: biomarkers, sampling, paper-based analytical devices, and perspectives, Analyst 147 (2022) 1273–1293, https://doi.org/10.1039/d1an01702k.
[2] C.-C. Tseng, C.-T. Kung, R.-F. Chen, M.-H. Tsai, H.-R. Chao, Y.-N. Wang, et al., Recent advances in microfluidic paper-based assay devices for diagnosis of human diseases using saliva, tears and sweat samples, Sensor. Actuator. B Chem. 342 (2021) 130078, https://doi.org/10.1016/j.snb.2021.130078.
[3] A. Himawan, L.K. Vora, A.D. Permana, S. Sudir, A.R. Nurdin, R. Nislawati, et al., Where microneedle meets biomarkers: futuristic application for diagnosing and monitoring localized external organ diseases, Adv. Healthcare Mater. 12 (2023) 2202066, https://doi.org/10.1002/adhm.202202066.
[4] R. Liu, A. Li, Y. Lang, H. Cai, X. Tang, D. Li, et al., Stimuli-responsive polymer microneedles: a rising transdermal drug delivery system and its applications in biomedical, J. Drug Deliv. Sci. Technol. 88 (2023) 104922, https://doi.org/10.1016/j.jddst.2023.104922.
[5] M. Friedel, I.A.P. Thompson, G. Kasting, R. Polsky, D. Cunningham, H.T. Soh, et al., Opportunities and challenges in the diagnostic utility of dermal interstitial fluid, Nat. Biomed. Eng. 7 (2023) 1541–1555, https://doi.org/10.1038/s41551-022-00998-9.
[6] Y. Cheng, X. Luan, J. Weng, L. Zhang, F. Ye, Engineering sampling microneedles for biomolecules sensing, Chem. Eng. J. 499 (2024) 156130, https://doi.org/10.1016/j.cej.2024.156130.
[7] A. Veronica, Y. Li, Y. Li, I.-M. Hsing, H.Y.Y. Nyein, Dermal-fluid-enabled detection platforms for non-invasive ambulatory monitoring, Sens Diagn 2 (2023) 1335–1359, https://doi.org/10.1039/D3SD00165B.
[8] A.M. Downs, A. Bolotsky, B.M. Weaver, H. Bennett, N. Wolff, R. Polsky, et al., Microneedle electrochemical aptamer-based sensing: Real-time small molecule measurements using sensor-embedded, commercially-available stainless steel microneedles, Biosens. Bioelectron. 236 (2023) 115408, https://doi.org/10.1016/j.bios.2023.115408.
[9] D.D. Zhu, Y.R. Tan, L.W. Zheng, J.Z. Lao, J.Y. Liu, J. Yu, et al., Microneedle-Coupled epidermal sensors for in-situ-multiplexed ion detection in interstitial fluids, ACS Appl. Mater. Interfaces (2023), https://doi.org/10.1021/acsami.3c00573.
[10] V. Schmitt, Sampling and Pharmacokinetics of Skin Interstitial Fluid for Therapeutically Monitored Drugs, University of British Columbia, 2015, https://doi.org/10.14288/1.0221674.
[11] T.K.L. Kiang, S.A. Ranamukhaarachchi, M.H.H. Ensom, Revolutionizing therapeutic drug monitoring with the use of interstitial fluid and microneedles technology, Pharmaceutics 9 (2017) 43, https://doi.org/10.3390/pharmaceutics9040043.
[12] R.L. Pereira, K.B. Vinayakumar, S. Sillankorva, Polymeric microneedles for health care monitoring: an emerging trend, ACS Sens. 9 (2024) 2294–2309, https://doi.org/10.1021/acssensors.4c00612.
[13] S. Pei, S. Babity, A. Sara Cordeiro, D. Brambilla, Integrating microneedles and sensing strategies for diagnostic and monitoring applications: the state of the art, Adv. Drug Deliv. Rev. 210 (2024) 115341, https://doi.org/10.1016/j.addr.2024.115341.

[14] Z. Wang, H. Li, J. Wang, Z. Chen, G. Chen, D. Wen, et al., Transdermal colorimetric patch for hyperglycemia sensing in diabetic mice, Biomaterials 237 (2020) 119782, https://doi.org/10.1016/j.biomaterials.2020.119782.
[15] J. Zhao, J. Lv, G. Ling, P. Zhang, A swellable hydrogel microneedle based on cerium-metal organic frame composite nanozyme for detection of biomarkers, Int. J. Biol. Macromol. 254 (2024) 127745, https://doi.org/10.1016/j.ijbiomac.2023.127745.
[16] J. Leanpolchareanchai, N. Nuchtavorn, Wearable microneedle-based colorimetric and fluorescence sensing for transdermal diagnostics, Talanta Open 8 (2023) 100247, https://doi.org/10.1016/j.talo.2023.100247.
[17] F. Ribet, A. Bendes, C. Fredolini, M. Dobielewski, M. Böttcher, O. Beck, et al., Microneedle patch for painless intradermal collection of interstitial fluid enabling multianalyte measurement of small molecules, SARS-CoV-2 antibodies, and protein profiling, Adv. Healthcare Mater. 12 (2023) 2202564, https://doi.org/10.1002/adhm.202202564.
[18] A. Mandal, An Alternative Diagnostic Method Using Microneedles for Sampling the Immune System in Situ. Thesis, Massachusetts Institute of Technology, 2017.
[19] Z. Bao, S. Lu, D. Zhang, G. Wang, X. Cui, G. Liu, Wearable microneedle patch for colorimetric detection of multiple signature biomarkers in vivo toward diabetic diagnosis, Adv. Healthcare Mater. 13 (2024) 2303511, https://doi.org/10.1002/adhm.202303511.
[20] Z. Li, Y. Wang, R. Zhang, Z. Liu, Z. Chang, Y. Deng, et al., Microneedles-based theranostic platform: from the past to the future, ACS Nano 18 (2024) 23876–23893, https://doi.org/10.1021/acsnano.4c04277.
[21] P.P. Samant, Microneedle Based Device to Sample Interstitial Fluid Through Skin, Georgia Institute of Technology, 2018. Phd Thesis.
[22] M. Tan, Y. Xu, Z. Gao, T. Yuan, Q. Liu, R. Yang, et al., Recent advances in intelligent wearable medical devices integrating biosensing and drug delivery, Adv. Mater. 34 (2022) 2108491, https://doi.org/10.1002/adma.202108491.
[23] P.R. Miller, R.J. Narayan, R. Polsky, Microneedle-based sensors for medical diagnosis, J. Mater. Chem. B 4 (2016) 1379–1383, https://doi.org/10.1039/C5TB02421H.
[24] N. Xu, W. Xu, M. Zhang, J. Yu, G. Ling, P. Zhang, Microneedle-based technology: toward minimally invasive disease diagnostics, Adv. Mater. Technol. 7 (2022) 2101595, https://doi.org/10.1002/admt.202101595.
[25] C.T. Sharkey, A.F. Aroche, I.G. Agusta, H. Nissan, T. Saha, S. Mukherjee, et al., Design and characterization of a self-powered microneedle microfluidic system for interstitial fluid sampling, Lab Chip 25 (2025) 4577–4587, https://doi.org/10.1039/D5LC00590F.
[26] J. Yang, J. Yang, X. Gong, Y. Zheng, S. Yi, Y. Cheng, et al., Recent progress in microneedles-mediated diagnosis, therapy, and theranostic systems, Adv Healthc Mater 11 (2022) e2102547, https://doi.org/10.1002/adhm.202102547.
[27] F. Amourizi, M. Ghaedi, Colorimetric determination of Mercury(II) by secondary gold nanoparticles formation on primary gold nanoparticles as an efficient nanozyme, Polyhedron 210 (2021) 115506, https://doi.org/10.1016/j.poly.2021.115506.
[28] S. Coppola, G. Nasti, V. Vespini, L. Mecozzi, R. Castaldo, G. Gentile, et al., Quick liquid packaging: encasing water silhouettes by three-dimensional polymer membranes, Sci. Adv. 5 (2019), https://doi.org/10.1126/sciadv.aat5189 eaat5189.
[29] C. Di Natale, S. Russo, F. Graziano, V. Vespini, G. Luciani, G. Vitiello, et al., Sensitive colorimetric immunosensor using AuNP-functionalized polymer film for picogram-level detection of tau protein intermediate aggregates, J. Colloid Interface Sci. 678 (2025) 1052–1059, https://doi.org/10.1016/j.jcis.2024.08.201.
[30] Z. Wang, L. Wu, M. Gerasimenko, T. Gilliland, Z.S.A. Shah, E. Lomax, et al., Seeding activity of skin misfolded tau as a biomarker for tauopathies, Mol. Neurodegener. 19 (2024) 92, https://doi.org/10.1186/s13024-024-00781-1.
[31] G.B. Frisoni, M. Boccardi, F. Barkhof, K. Blennow, S. Cappa, K. Chiotis, et al., Strategic roadmap for an early diagnosis of Alzheimer's disease based on biomarkers, Lancet Neurol. 16 (2017) 661–676, https://doi.org/10.1016/S1474-4422(17)30159-X.
[32] L. Zhang, K. Cao, Y. Su, S. Hu, X. Liang, Q. Luo, et al., Colorimetric and surface-enhanced raman scattering dual-mode magnetic immunosensor for ultrasensitive detection of blood phosphorylated tau in Alzheimer's disease, Biosens. Bioelectron. 222 (2023) 114935, https://doi.org/10.1016/j.bios.2022.114935.
[33] L.M.T. Phan, S. Cho, Fluorescent aptasensor and colorimetric aptablot for p-tau231 detection: toward early diagnosis of alzheimer's disease, Biomedicines 10 (2022) 93, https://doi.org/10.3390/biomedicines10010093.
[34] F. Amourizi, K. Dashtian, R. Zare-Dorabei, S. Hajati, Transformative personalized oxalate biomarker analysis through a wrist-worn microneedle device integrated with duplex nanozyme toolbox, Sensor. Actuator. B Chem. 423 (2025) 136731, https://doi.org/10.1016/j.snb.2024.136731.
[35] DM dos Santos, K. Khachornsakkul, S. Sonkusale, Microneedle-integrated distance-based paper device for simultaneous transdermal detection of cortisol and dopamine, Lab Chip 25 (2025) 2708–2721, https://doi.org/10.1039/D4LC00983E.
[36] A. Luchini, G. D'Errico, S. Leone, Z. Vaezi, A. Bortolotti, L. Stella, et al., Structural organization of lipid-functionalized-au nanoparticles, Colloids Surf. B Biointerfaces 168 (2018) 2–9, https://doi.org/10.1016/j.colsurfb.2018.04.044.
[37] M. Gaur, S. Maurya, M.S. Akhtar, A.B. Yadav, Synthesis and evaluation of BSA-loaded PLGA-chitosan composite nanoparticles for the protein-based drug delivery system, ACS Omega 8 (2023) 18751–18759, https://doi.org/10.1021/acsomega.3c00738.
[38] K. Manickam, R.R. Machireddy, S. Seshadri, Characterization of biomechanical properties of agar based tissue mimicking phantoms for ultrasound stiffness imaging techniques, J. Mech. Behav. Biomed. Mater. 35 (2014) 132–143, https://doi.org/10.1016/j.jmbbm.2014.03.017.
[39] S. Diridollou, F. Patat, F. Gens, L. Vaillant, D. Black, J.M. Lagarde, et al., In vivo model of the mechanical properties of the human skin under suction, Skin Res. Technol. 6 (2000) 214–221, https://doi.org/10.1034/j.1600-0846.2000.006004214.x.
[40] J. Sun, Y. Lu, L. He, J. Pang, F. Yang, Y. Liu, Colorimetric sensor array based on gold nanoparticles: design principles and recent advances, TrAC, Trends Anal. Chem. 122 (2020) 115754, https://doi.org/10.1016/j.trac.2019.115754.
[41] L. Yu, Z. Song, J. Peng, M. Yang, H. Zhi, H. He, Progress of gold nanomaterials for colorimetric sensing based on different strategies, TrAC, Trends Anal. Chem. 127 (2020) 115880, https://doi.org/10.1016/j.trac.2020.115880.
[42] N.A. Masdor, Determination of the detection limit using the four-parameter logistic model for the double-antibody sandwich ELISA for the rapid detection of Bacillus cereus in food, J Environ Microbiol Toxicol 5 (2017) 12–13, https://doi.org/10.54987/jemat.v5i1.415.
[43] M.A. O'Connell, B.A. Belanger, P.D. Haaland, Calibration and assay development using the four-parameter logistic model, Chemometr. Intell. Lab. Syst. 20 (1993) 97–114, https://doi.org/10.1016/0169-7439(93)80008-6.
[44] K.-H. Ke, C.-K. Chung, High-performance Al/PDMS TENG with novel complex morphology of two-height microneedles array for high-sensitivity force-sensor and self-powered application, Small 16 (2020) 2001209, https://doi.org/10.1002/smll.202001209.
[45] W. Xiong, F. Zhang, S. Qu, L. Yin, K. Li, Y. Huang, Marangoni-driven deterministic formation of softer, hollow microstructures for sensitivity-enhanced tactile system, Nat. Commun. 15 (2024) 5596, https://doi.org/10.1038/s41467-024-49864-z.
[46] C.D. Natale, D.D. Rosa, M. Profeta, R. Jamaledin, A. Attanasio, E. Lagreca, et al., Design of biodegradable bi-compartmental microneedles for the stabilization and the controlled release of the labile molecule collagenase for skin healthcare, J. Mater. Chem. B 9 (2021) 392–403, https://doi.org/10.1039/D0TB02279A.
[47] S. Coppola, V. Vespini, G. Nasti, P. FerraroTransmitting light through biocompatible and biodegradable drug delivery micro needlesIEEE Journal of Selected Topics in Quantum Electronics 27520201810.1109/JSTQE.2021.3057834.
[48] V. Onesto, C. Di Natale, M. Profeta, P.A. Netti, R. Vecchione, Engineered PLGA-PVP/VA based formulations to produce electro-drawn fast biodegradable microneedles for labile biomolecule delivery, Prog. Biomater. 9 (2020) 203–217, https://doi.org/10.1007/s40204-020-00143-2.
[49] C. Di Natale, V. De Gregorio, E. Lagreca, F. Mauro, B. Corrado, R. Vecchione, et al., Engineered bacterial cellulose nanostructured matrix for incubation and release of drug-loaded oil in water nanoemulsion, Front. Bioeng. Biotechnol. 10 (2022), https://doi.org/10.3389/fbioe.2022.851893.
[50] D.A. Armbruster, T. Pry, Limit of blank, limit of detection and limit of quantitation, Clin. Biochem. Rev. 29 (2008) S49–S52.
[51] A.F. Moreira, C.F. Rodrigues, T.A. Jacinto, S.P. Miguel, E.C. Costa, I.J. Correia, Poly (vinyl alcohol)/chitosan layer-by-layer microneedles for cancer chemo-photothermal therapy, Int. J. Pharm. 576 (2020) 118907, https://doi.org/10.1016/j.ijpharm.2019.118907.
[52] D. Zhang, D.B. Das, C.D. Rielly, Microneedle assisted micro-particle delivery from gene guns: experiments using skin-mimicking agarose gel, J. Pharmaceut. Sci. 103 (2014) 613–627, https://doi.org/10.1002/jps.23835.